



This is a repository copy of *Traction Forces of Endothelial Cells under Slow Shear Flow*.

White Rose Research Online URL for this paper:  
<http://eprints.whiterose.ac.uk/91052/>

Version: Accepted Version

---

**Article:**

Perrault, C., Brugues, A., Bazellieres, E. et al. (3 more authors) (2015) Traction Forces of Endothelial Cells under Slow Shear Flow. *Biophysical Journal*, 109 (8). pp. 1533-1536. ISSN 0006-3495

<https://doi.org/10.1016/j.bpj.2015.08.036>

---

Article available under the terms of the CC-BY-NC-ND licence  
(<https://creativecommons.org/licenses/by-nc-nd/4.0/>)

**Reuse**

Unless indicated otherwise, fulltext items are protected by copyright with all rights reserved. The copyright exception in section 29 of the Copyright, Designs and Patents Act 1988 allows the making of a single copy solely for the purpose of non-commercial research or private study within the limits of fair dealing. The publisher or other rights-holder may allow further reproduction and re-use of this version - refer to the White Rose Research Online record for this item. Where records identify the publisher as the copyright holder, users can verify any specific terms of use on the publisher's website.

**Takedown**

If you consider content in White Rose Research Online to be in breach of UK law, please notify us by emailing [eprints@whiterose.ac.uk](mailto:eprints@whiterose.ac.uk) including the URL of the record and the reason for the withdrawal request.



[eprints@whiterose.ac.uk](mailto:eprints@whiterose.ac.uk)  
<https://eprints.whiterose.ac.uk/>

## Biophysical Letter

### Traction Forces of Endothelial Cells under Slow Shear Flow

Cecile M. Perrault,<sup>1,2,3,\*</sup> Agusti Brugues,<sup>3</sup> Elsa Bazellieres,<sup>3</sup> Pierre Ricco,<sup>2</sup> Damien Lacroix,<sup>1,2,3</sup> and Xavier Trepap<sup>3,4,5,6</sup>

<sup>1</sup>Institute for In Silico Medicine and <sup>2</sup>Department of Mechanical Engineering, University of Sheffield, Sheffield, United Kingdom; <sup>3</sup>Institute for Bioengineering of Catalonia, Barcelona, Spain; <sup>4</sup>Facultat de Medicina, Universitat de Barcelona, Barcelona, Spain; <sup>5</sup>Centro de Investigación Biomédica en Red en Bioingeniería, Biomateriales y Nanomedicina, Barcelona, Spain; and <sup>6</sup>Institució Catalana de Recerca i Estudis Avançats, Barcelona, Spain

**ABSTRACT** Endothelial cells are constantly exposed to fluid shear stresses that regulate vascular morphogenesis, homeostasis, and disease. The mechanical responses of endothelial cells to relatively high shear flow such as that characteristic of arterial circulation has been extensively studied. Much less is known about the responses of endothelial cells to slow shear flow such as that characteristic of venous circulation, early angiogenesis, atherosclerosis, intracranial aneurysm, or interstitial flow. Here we used a novel, to our knowledge, microfluidic technique to measure traction forces exerted by confluent vascular endothelial cell monolayers under slow shear flow. We found that cells respond to flow with rapid and pronounced increases in traction forces and cell-cell stresses. These responses are reversible in time and do not involve reorientation of the cell body. Traction maps reveal that local cell responses to slow shear flow are highly heterogeneous in magnitude and sign. Our findings unveil a low-flow regime in which endothelial cell mechanics is acutely responsive to shear stress.

Received for publication 4 March 2015 and in final form 11 August 2015.

\*Correspondence: [c.perrault@sheffield.ac.uk](mailto:c.perrault@sheffield.ac.uk)

The ability of endothelial cells (ECs) to sense and adapt to shear flow is one of the best-studied phenomena in all mechanobiology. In response to flow, ECs are known to change their orientation, remodel cell-cell and cell-matrix adhesions, modify patterns of gene expression, and alter protein localization at the cell membrane (1). Because these responses are downstream of a mechanical stimulus, a number of studies have analyzed the time evolution of cell-matrix tractions during the application of shear flow. Some of these studies reported increases in traction forces with shear flow (2–4), whereas others reached the opposite conclusion (5,6).

Previous studies of traction forces exerted by ECs in the presence of constant shear flow focused on the application of shear stresses  $>1$  Pa ( $10$  dyn/cm<sup>2</sup>). Shear stresses in this range are characteristic of arterial flow during physiological function. In many other physiological and pathological conditions, however, shear stresses are much weaker. This is the case of shear stresses during venous (7) and interstitial flow (8), as well as during atherosclerosis (9) and intracranial aneurysm (10). The biochemical and structural responses of ECs to high versus low shear stress have been extensively shown to differ in terms of cell morphology, orientation, and expression of vasoactive agents, antioxidant enzymes, growth regulators, inflammatory mediators, and adhesion molecules (reviewed by Malek et al. (9)). Moreover, in the presence of ultraslow flow such as interstitial flow (11), ECs are capable of forming numerous capillary-like structures and have a greater rate of invasion (12). Many of the phenomena described above are likely to involve a synergy

between flow sensing and force generation (13), but the link between slow flow and cell contractility is unknown.

To address this question, we combined traction microscopy (TM) and monolayer stress microscopy (MSM) with microfluidic techniques and explored cellular traction forces in reaction to slow shear flow (Fig. 1). TM maps the magnitude, location, and direction of the forces exerted by cells against their underlying soft substrate (14). Substrate displacements caused by cell tractions are mapped using fiducial markers embedded in the soft substrate. The displacement fields are then used to compute tractions by inverting the elasticity equations in Fourier space.

TM was integrated into a microfluidic chamber, created in PDMS (polydimethylsiloxane) by soft lithography. A mold was machined from Plexiglas to create rectangular flow channel of 2 mm in width and 2 cm in length. The channel was designed to have two different heights over its length, thus creating a channel with two different shear stress values (15). The circulating media entered a chamber with an initial height of 300  $\mu$ m, and moved into a chamber with a height of 600  $\mu$ m. Corresponding shear stress values can be found in Table S1 in the Supporting Material. Cell tractions were monitored in both chambers, away from the transition zone between the two.

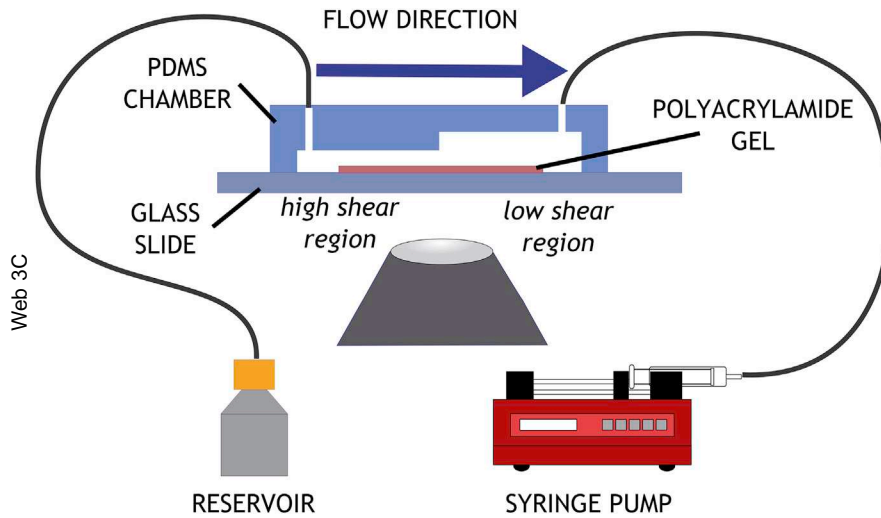


**FIGURE 1** Microfluidic traction assay. A PDMS flow chamber is assembled over a strip of polyacrylamide ( $E = 1.25$  KPa) polymerized on a glass coverslip. The chamber is divided into two sections of varying heights. The flow is controlled by a syringe pump. To see this figure in color, go online.

Monolayers of human umbilical vein endothelial cells were exposed to a time-varying protocol alternating no-flow and applied flow in the range 0.014–0.133 Pa (see Fig. 2 and the Supporting Material). The temporal stress pattern consisted of two consecutive flow steps of 30-min duration and increasing magnitude (5 and 10 mL/h), followed by a 30-min period of no flow. After this period, we applied a second pulse of flow (10 mL/h) lasting 30 min.

Upon exposure to flow, we observed an acute increase in strain energy (the total energy transmitted by the cells on the substrate) with no significant differences between the two flow levels (Fig. 2). Subsequent doubling of the shear flow did not trigger a second increase in traction forces. Instead, cells tended to plateau at values that were 50–100% higher than baseline levels. Quickly after stopping the flow, the strain energy relaxed toward baseline levels, thus indicating reversibility of responses to flow. Applica-

tion of an additional flow pulse triggered a second acute increase in tractions, with pronounced differences between the two flow levels, which is suggestive of a memory effect. Finally, stopping the flow led to a relaxation toward baseline levels.

The responses shown in Fig. 2 are spatial averages of traction maps. As previously shown in a diversity of cell types (6,16), these maps exhibited a punctate distribution with large spatial heterogeneities (Fig. 3, A and B). The response to shear flow was also heterogeneous; although the overall traction of the monolayer increased, several cells displayed significant traction drops (Fig. 3 C). The magnitude of local changes in traction in response to shear was similar to the global traction average. Upon flow application, tractions showed a weak but significant tendency to orient perpendicular to the direction of flow ( $p < 0.001$ , Rayleigh test, Fig. 3, D and E).

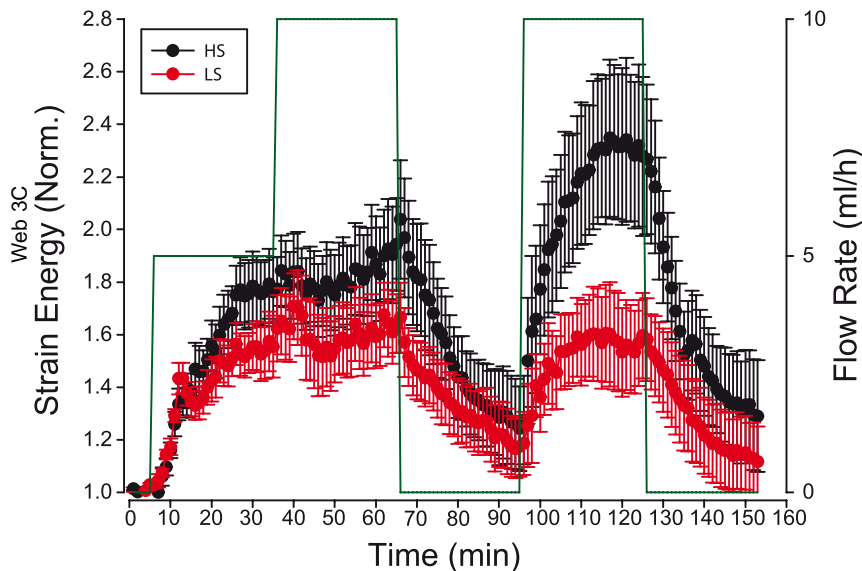
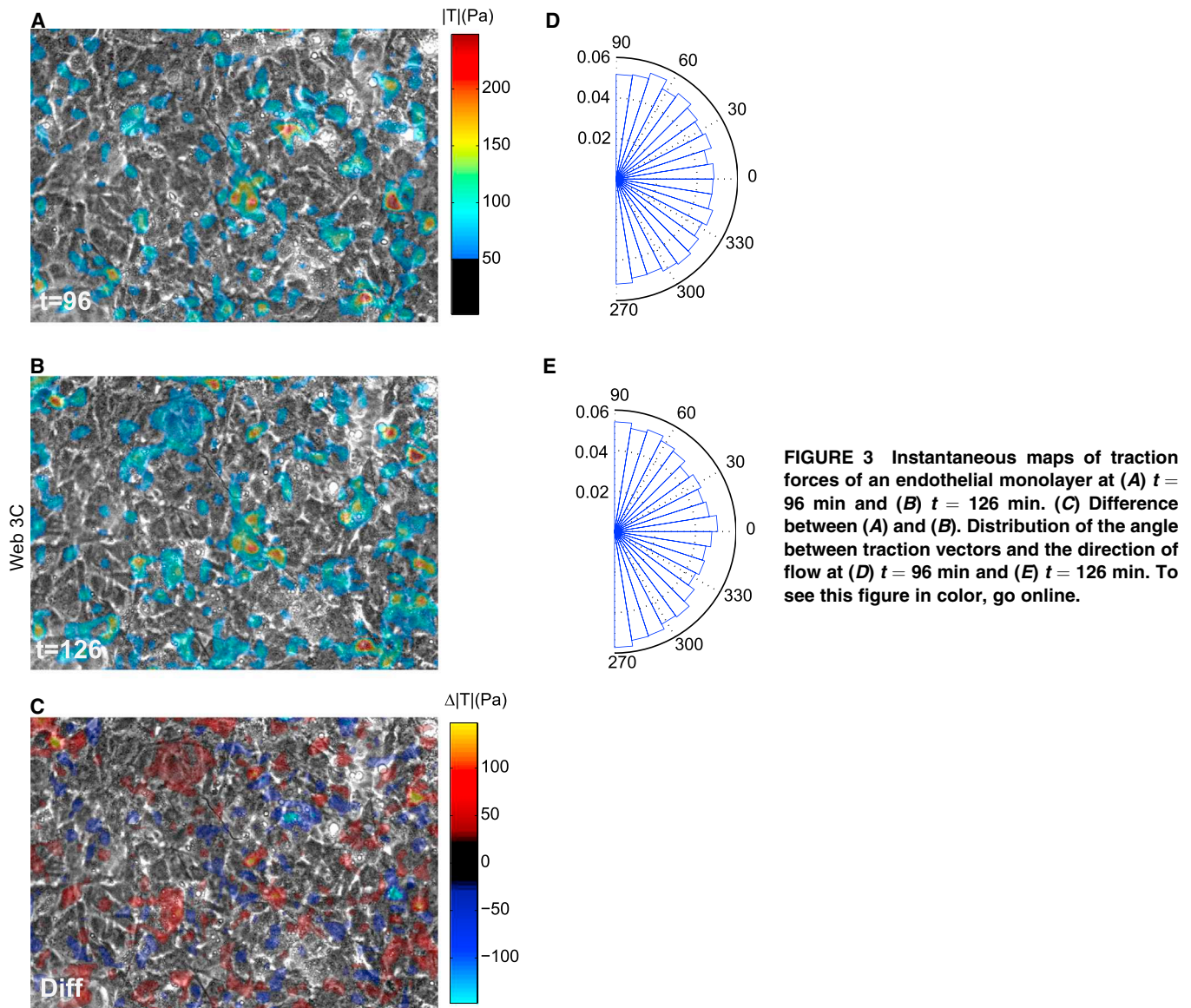


**FIGURE 2** ECs display acute responses to slow shear flow. Strain energy was normalized to its baseline ( $t = 0$ ). (Green line) Flow values. (Red and black lines) High shear (HS) stress and low shear (LS) stress; both shear stresses were at least one order-of-magnitude lower than previously reported shear stresses in TM experiments.  $n = 6$  monolayers per condition. Differences between HS and LS are only significant during the second shear pulse ( $t = 105$  min and  $t = 125$  min,  $p \leq 0.05$ ). The slopes of the strain energy between the first and second flow periods were not significant. To see this figure in color, go online.



Finally, we used MSM to measure cell-cell stresses (14). As reported previously (6,14), cell-cell stresses showed supracellular spatial fluctuations (see Fig. S1). Upon flow application, these fluctuations increased in magnitude but cell-cell stresses did not change in orientation. Unlike cell-substrate tractions, cell-cell stresses did not show significant differences depending on flow magnitude.

Traction forces in the presence of constant shear stresses of relatively high magnitude ( $>1$  Pa) have been extensively characterized in previous studies, with conflicting results (2–6). Here we used shear stresses between one and two orders-of-magnitude smaller than those applied in previous studies based on TM. In response to these low stresses, ECs exhibited acute but reversible increases in traction. These responses were fast and more pronounced than those reported in previous studies using higher shear flows (2–6). The low

shear stresses applied here fall within the range of physiological interstitial flow (8). Because interstitial flow induces angiogenesis, we speculate that increased traction forces observed here might recapitulate those required to initiate the formation of new blood vessels in vivo (17). Low flows are also characteristic of pathological conditions such as intracranial aneurysm (10) and atherosclerosis (9); our findings raise the question of whether increases in traction forces might be protective or disruptive in these conditions.

A remarkable feature of our experiments was the heterogeneity of the responses. Heterogeneous responses of ECs to flow have been previously reported (18) in terms of protein and mRNA levels, calcium signaling, and organelle localization. Heterogeneity has been attributed to the topography of the monolayer (19), the heterogeneous location, properties of cytoskeleton elements (20), and flow sensors. Our

findings of heterogeneous force distributions might underlie heterogeneous responses in signaling and molecular localization through mechanotransduction activity. Whether such activity is dominated by cell-matrix or cell-cell stresses could be elicited based on the differences in the characteristic lengths of the corresponding fluctuations.

In conclusion, we used a new device, to our knowledge, to combine microfluidics, TM, and MSM to assess the mechanical response of ECs to slow shear flow. The observed acute increases in traction generation provide fresh insights into the synergy between flow and the biomechanical reaction of cells, with potential implications in morphogenesis and disease.

## SUPPORTING MATERIAL

Supporting Materials and Methods, one table, and one figure, are available at [http://www.biophysj.org/biophysj/supplemental/S0006-3495\(15\)00871-1](http://www.biophysj.org/biophysj/supplemental/S0006-3495(15)00871-1).

## AUTHOR CONTRIBUTIONS

C.M.P., D.L., and X.T. designed the study; C.M.P. implemented the flow chamber and carried out experiments; C.M.P., A.B., and E.B. processed data; C.M.P. and X.T. wrote the article; P.R. calculated shear and gel displacement in the chamber; and all authors discussed and interpreted results and commented on the article.

## ACKNOWLEDGMENTS

We thank Daniel Navajas, and members of the Integrative Cell and Tissue Dynamics Lab and the MechanoBio Lab at the Institute for Bioengineering of Catalonia, for fruitful discussions.

C.M.P. received funding from the Institute for Bioengineering of Catalonia. This work was funded by the Spanish Ministry of Economy and Competitiveness (under grant No. BFU2012-38146), the Generalitat de Catalunya (under grant No. 2014-SGR-927), and the European Research Council (under grant No. CoG-616480).

## SUPPORTING CITATIONS

References (21–24) appear in the [Supporting Material](#).

## REFERENCES

1. Davies, P. F. 1995. Flow-mediated endothelial mechanotransduction. *Physiol. Rev.* 75:519–560.
2. Hur, S. S., J. C. del Álamo, ..., S. Chien. 2012. Roles of cell confluency and fluid shear in 3-dimensional intracellular forces in endothelial cells. *Proc. Natl. Acad. Sci. USA.* 109:11110–11115.
3. Shiu, Y.-T., S. Li, ..., S. Chien. 2004. Rho mediates the shear-enhancement of endothelial cell migration and traction force generation. *Bio-phys. J.* 86:2558–2565.

4. Ting, L. H., J. R. Jahn, ..., N. J. Sniadecki. 2012. Flow mechanotransduction regulates traction forces, intercellular forces, and adherens junctions. *Am. J. Physiol. Heart Circ. Physiol.* 302:H2220–H2229.
5. Conway, D. E., M. T. Breckenridge, ..., M. A. Schwartz. 2013. Fluid shear stress on endothelial cells modulates mechanical tension across VE-cadherin and PECAM-1. *Curr. Biol.* 23:1024–1030.
6. Steward, R., D. Tambe, ..., J. J. Fredberg. 2015. Fluid shear, intercellular stress, and endothelial cell alignment. *Am. J. Physiol. Cell Physiol.* Published online February 4, 2015. <http://dx.doi.org/10.1152/ajpcell.00363.2014>.
7. Wragg, J. W., S. Durant, ..., R. Bicknell. 2014. Shear stress regulated gene expression and angiogenesis in vascular endothelium. *Microcirculation.* 21:290–300.
8. Swartz, M. A., and M. E. Fleury. 2007. Interstitial flow and its effects in soft tissues. *Annu. Rev. Biomed. Eng.* 9:229–256.
9. Malek, A. M., S. L. Alper, and S. Izumo. 1999. Hemodynamic shear stress and its role in atherosclerosis. *J. Amer. Med. Assoc.* 282:2035–2042.
10. Meng, H., V. M. Tutino, ..., A. Siddiqui. 2014. High WSS or low WSS? Complex interactions of hemodynamics with intracranial aneurysm initiation, growth, and rupture: toward a unifying hypothesis. *Am. J. Neuroradiol.* 35:1254–1262.
11. Park, J. Y., J. B. White, ..., S. Takayama. 2011. Responses of endothelial cells to extremely slow flows. *Biomicrofluidics.* 5:22211.
12. Song, J. W., and L. L. Munn. 2011. Fluid forces control endothelial sprouting. *Proc. Natl. Acad. Sci. USA.* 108:15342–15347.
13. Kniazeva, E., and A. J. Putnam. 2009. Endothelial cell traction and ECM density influence both capillary morphogenesis and maintenance in 3-D. *Am. J. Physiol. Cell Physiol.* 297:C179–C187.
14. Tambe, D. T., C. C. Hardin, ..., X. Trepat. 2011. Collective cell guidance by cooperative intercellular forces. *Nat. Mater.* 10:469–475.
15. Galie, P. A., A. van Oosten, ..., P. A. Janmey. 2015. Application of multiple levels of fluid shear stress to endothelial cells plated on polyacrylamide gels. *Lab Chip.* 15:1205–1212.
16. Trepat, X., M. R. Wasserman, ..., J. J. Fredberg. 2009. Physical forces during collective cell migration. *Nat. Phys.* 5:426–430.
17. Hernández Vera, R., E. Genové, ..., C. E. Semino. 2009. Interstitial fluid flow intensity modulates endothelial sprouting in restricted Src-activated cell clusters during capillary morphogenesis. *Tissue Eng. A.* 15:175–185.
18. Davies, P. F., T. Mundel, and K. A. Barbee. 1995. A mechanism for heterogeneous endothelial responses to flow in vivo and in vitro. *J. Biomech.* 28:1553–1560.
19. Barbee, K. A. 2002. Role of subcellular shear-stress distributions in endothelial cell mechanotransduction. *Ann. Biomed. Eng.* 30:472–482.
20. Davies, P. F., J. Zilberberg, and B. P. Helmke. 2003. Spatial microstimuli in endothelial mechanosignaling. *Circ. Res.* 92:359–370.
21. Kandow, C. E., P. C. Georges, ..., K. A. Benigno. 2007. Polyacrylamide hydrogels for cell mechanics: steps toward optimization and alternative uses. *Methods Cell Biol.* 83:29–46.
22. White, F. M. 2003. Fluid Mechanics. McGraw-Hill, New York.
23. Yeung, T., P. C. Georges, ..., P. A. Janmey. 2005. Effects of substrate stiffness on cell morphology, cytoskeletal structure, and adhesion. *Cell Motil. Cytoskeleton.* 60:24–34.
24. Tambe, D. T., U. Croutelle, ..., J. J. Fredberg. 2013. Monolayer stress microscopy: limitations, artifacts, and accuracy of recovered intercellular stresses. *PLoS One.* 8:e55172.

# TRACTION FORCES OF ENDOTHELIAL CELLS UNDER SLOW SHEAR FLOW

C.M. Perrault<sup>1,2,3</sup>, A. Brugués<sup>3</sup>, E. Bazellieres<sup>3</sup>, P. Ricco<sup>2</sup>, D. Lacroix<sup>1,2,3</sup> and X. Trepât<sup>3,4,5</sup>

<sup>1</sup>INSIGNEO Institute for in-silico Medicine, University of Sheffield, Sheffield, UK; <sup>2</sup>Department of Mechanical Engineering, University of Sheffield, Sheffield, UK; <sup>3</sup>Institute for Bioengineering of Catalonia, Barcelona, Spain; <sup>4</sup>Facultat de Medicina, Universitat de Barcelona, and Ciber-BBN, Barcelona, Spain; <sup>5</sup>Institució Catalana de Recerca i Estudis Avançats, Barcelona, Spain.

## Supplementary material

### 1. Materials and Methods

#### 1.1. Preparation of polyacrylamide gels and cell culture

Large rectangular coverslips were activated by using a 1:1:14 solution of acetic acid/bind-silane/ethanol. The dishes were washed twice with ethanol and air-dried for 10 min.

Polyacrylamide gels ( $E = 1.25$  kPa) were prepared as described in Kadow et al (1) and Yeung et al (2). Briefly, a solution containing 5% acrylamide, 0.1% bis acrylamide, 0.5% ammonium persulphate, 0.05% tetramethylethylenediamine, 0.4% of 200-nm-diameter red fluorescent carboxylate-modified beads and 2 mg ml<sup>-1</sup> NH-acrylate was prepared. A molding channel was created on the coverslip using double sided-tape and transparency paper to create polyacrylamide gels with dimensions of 1mm in width and 2cm in length. A drop of 10  $\mu$ l was placed on one end of the channel, which then fills by capillary action.

After polymerization, tape and paper were carefully removed and the gels were washed with PBS and incubated with 100 $\mu$ l of a collagen I solution (0.1 mg/ml, Millipore) overnight at 4°C. The gels were washed afterwards with PBS and cells were seeded and incubated with cell culture media with 10% FBS for 6h.

HUVEC cells were cultured in EGM<sup>TM</sup> BulletKit<sup>TM</sup> (Lonza, MA).

#### 1.2. Flow experiments

A small volume (8  $\mu$ l) containing 150,000 cells was placed on the polyacrylamide gel. Once the cells were attached to the polyacrylamide gel (20 min), the unattached cells were washed away and 2 ml of medium were added. Twelve hours after seeding the cells, the coverslip was attached to the PDMS flow chamber and held together by a custom-made holder. The ensemble was then placed on the microscope and connected on one side to a syringe pump (World Precision Instruments Aladdin 1000, WPI, FL) and to the other side to a reservoir of degassed medium.

#### 1.3. Time-lapse microscopy

Multidimensional acquisition routines were performed on an automated inverted microscope (Nikon Eclipse Ti) equipped with thermal, CO<sub>2</sub> and humidity control, using MetaMorph (Universal Imaging)

software. Time-lapse recording started approximately 10 min after assembly. The interval between image acquisition was 1 min.

#### 1.4. Traction microscopy (TM)

Cell tractions were evaluated using monolayer Fourier-transform traction microscopy (3). Briefly, the displacement field was calculated by comparing fluorescent microbead images obtained during the experiment with a reference image taken at the end of the experiment after the trypsinization and the consequent detachment of the cells from the underlying substrate. A particle imaging velocimetry algorithm (3) was used to determine the deformation of the substrate caused by the traction forces.

#### 1.5 Monolayer Stress Microscopy (MSM)

In a 2D approximation, monolayer stress is fully captured by a tensor possessing two independent normal components ( $\sigma_{xx}$  and  $\sigma_{yy}$ ) and two identical shear components ( $\sigma_{xy}$  and  $\sigma_{yx}$ ). At every pixel of the monolayer, these four components of the stress tensor define two particular directions of the plane, one in which the normal stress is maximum and one in which it is minimum. These directions, which are mutually orthogonal, are called principal stress orientations, and the stress values in each principal orientation are called maximum ( $\sigma_{11}$ ) and minimum ( $\sigma_{22}$ ) stress components. The average normal stress is defined as  $\sigma_{avg}=(\sigma_{11}+\sigma_{22})/2$ , while the maximum shear stress is defined as  $\sigma_s=(\sigma_{11}-\sigma_{22})/2$ . The spatial resolution and force precision of MSM are formally set by those in the original traction maps. How the reconstructed stress field is affected by the choice of boundary conditions and by the assumptions of continuity, incompressibility, and homogeneity was extensively studied elsewhere (3,6).

#### 1.6 Statistical analysis

Summary data are expressed as mean  $\pm$  SEM (standard error of the mean). Unless noted otherwise, statistical comparisons were computed by Student's t-test. Traction angles were compared to an isotropic distribution using a Raleigh test. A value of  $p \leq 0.05$  was considered statistically significant.

## 2. Flow analysis in the microfluidic chamber

The microfluidic chamber was created to limit contact of the cells with PDMS prior to the experiment. As a result, the system was designed with two components: 1) a strip of PAA gels on a glass slide and 2) the PDMS flow chamber. To maintain both sides together during operation, a customized aluminium holder was created to apply mechanical forces over the assembly. To facilitate alignment and limit leakage, the PAA gels were created slightly less wide than the flow channel, but the gap was small enough to avoid fluctuations in the fluid distribution, as observed by flow of fluorescent beads.

To ensure that the displacement of the beads in the polyacrylamide gels was only caused by the cells, the displacement of the upper layer of the gels due to shear stress was calculated. As the Reynolds number of the flow ( $Re = u d v^{-1}$ , where  $u$  is the velocity,  $d$  is the hydraulic diameter and  $v$  is the kinematic viscosity) is low, the flow can be assumed to be laminar. Assuming Poiseuille flow, the flow rate per unit width ( $m^2/s$ ) is related to the streamwise mean pressure gradient as follows (4):

$$Q = \frac{2P_x d^3}{3\mu} \quad (1)$$

Where  $P_x$  represents the pressure gradient along the streamwise direction and  $\mu$  is the viscosity of the fluid.

As the flow rate per unit width is related to the volumetric flow rate  $Q_{vol} = Q \times w$ , the pressure gradient is readily found. The laminar flow is given by

$$u = \frac{P_x}{2\mu} (d^2 - y^2) \quad (2)$$

where the  $y$  coordinate is taken from the middle of the gap so that the wall-shear stress  $\tau_w$  is found

$$\tau_w = \mu \left. \frac{du}{dy} \right|_{y=-d} = P_x d \quad (3)$$

The angle  $\gamma$  of deformation of the surface is

$$\gamma = \frac{\tau_w}{G} \quad (4)$$

where  $G$  is the shear modulus of the flexible surface.

The streamwise displacement  $\Delta s$  of the flexible surface is thus

$$\Delta s = h \tan(\gamma) \quad (5)$$

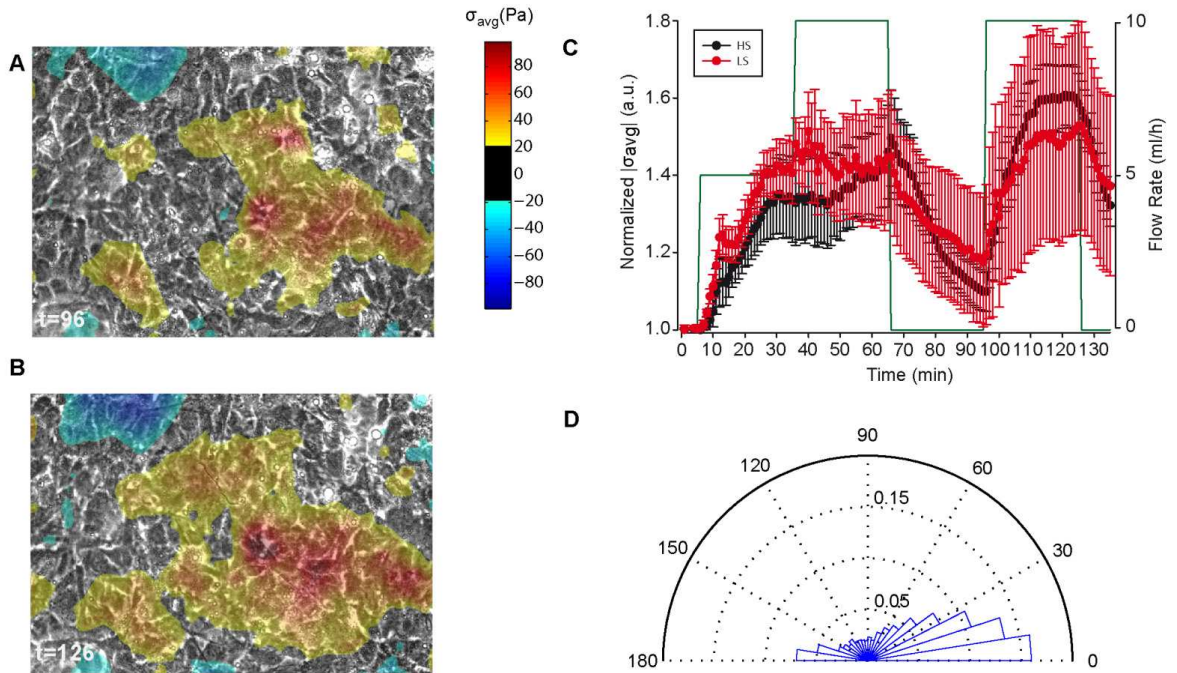
The results for flow rates of 5 and 10 mL/hr in the small and large region of the chambers are summarized in the table 1.

	Small chamber (high shear)		Large chamber (low shear)	
	Wall shear stress	Gel displacement	Wall shear stress	Gel displacement
Q= 5mL/hr	0.066 Pa	$2.7 \times 10^{-9}$ m	0.014 Pa	$5.5 \times 10^{-10}$ m
Q= 10 mL/hr	0.133 Pa	$5.3 \times 10^{-9}$ m	0.028 Pa	$1.1 \times 10^{-9}$ m

**Table 1. Wall shear stress and gel displacement values for the flow rates applied during the experiments in both chambers of the flow device. Gel stiffness is 1.25kPa.**

The displacement of the gel due to the flow is thus minimal and the shear stress values correspond to a low flow regime (5).

### 3. Supplementary Figure



Supplementary Fig S1. Cell-cell stresses display acute and reversible responses to low shear flow. A-B) Maps of the average normal stress at  $t=96$  min and  $t=126$  min (same time points as in Fig. 3 in the main text). C) Time evolution of the average cell-cell stresses (norm of the average normal stress) in response to the flow pattern depicted in green ( $n=6$  per condition). D) Angular change of the maximum principal stress between  $t=96$  min and  $t=126$  min. These data show that changes in cell-cell stress orientation in response to shear flow were minimal.

#### SUPPORTING REFERENCES

1. Kadow, C.E., P.C. Georges, P.A. Janmey, and K.A. Beningo. 2007. Polyacrylamide hydrogels for cell mechanics: steps toward optimization and alternative uses. *Methods Cell Biol.* 83: 29–46.
2. Yeung, T., P.C. Georges, L.A. Flanagan, B. Marg, M. Ortiz, M. Funaki, N. Zahir, W. Ming, V. Weaver, and P.A. Janmey. 2005. Effects of substrate stiffness on cell morphology, cytoskeletal structure, and adhesion. *Cell Motil. Cytoskeleton.* 60: 24–34.
3. Tambe, D.T., C.C. Hardin, T.E. Angelini, K. Rajendran, C.Y. Park, X. Serra-Picamal, E.H. Zhou, M.H. Zaman, J.P. Butler, D.A. Weitz, J.J. Fredberg, and X. Trepat. 2011. Collective cell guidance by cooperative intercellular forces. *Nat. Mater.* 10: 469–75.
4. White, F.M. 2003. *Fluid Mechanics*. McGraw-Hill.
5. Swartz, M.A., and M.E. Fleury. 2007. Interstitial flow and its effects in soft tissues. *Annu. Rev. Biomed. Eng.* 9: 229–56.
6. Tambe DT, Croutelle U, Trepat X, Park CY, Kim JH, Millet E, Butler JP, and Fredberg JJ. Monolayer stress microscopy: limitations, artifacts, and accuracy of recovered intercellular stresses. *PloS one* 8, e55172 (2013).